Fabrication of Fe_3O_4-incorporated MnO_2 nanoflowers as electrodes for enhanced asymmetric supercapacitor performance

Iqra Rabani[a], Ayesha Younus[b], Supriya Patil[a], and Young-Soo Seo[a*]

[a]Department of Nanotechnology and Advanced Materials Engineering, Sejong University, Seoul 05006, Republic of Korea

[b]Department of Physics, University of Agriculture, Faisalabad 38000, Pakistan

*Corresponding author E-mail: ysseo@sejong.ac.kr

Figure Content

Figure S1. N_2 ads/des isotherms of the pristine Fe_3O_4, pristine MnO_2 and MnO_2@Fe_3O_4 nanoflower like structure.

Figure S2. BJH curves of the pristine Fe_3O_4, pristine MnO_2 and MnO_2@Fe_3O_4 nanoflower like structure.

Figure S3. Nyquist plot of the Fe_3O_4, MnO_2 and MnO_2@Fe_3O_4 nanoflowers.

Figure S4. CV for the activated carbon for the Fe_3O_4 at various scan rates in the potential range from -1.0 V to 0 V.

S5. **Calculations for the loading mass**

Table S1. Comparison of specific capacitance of MnO_2@Fe_3O_4 nanoflowers reported to date with those in the present study.

References

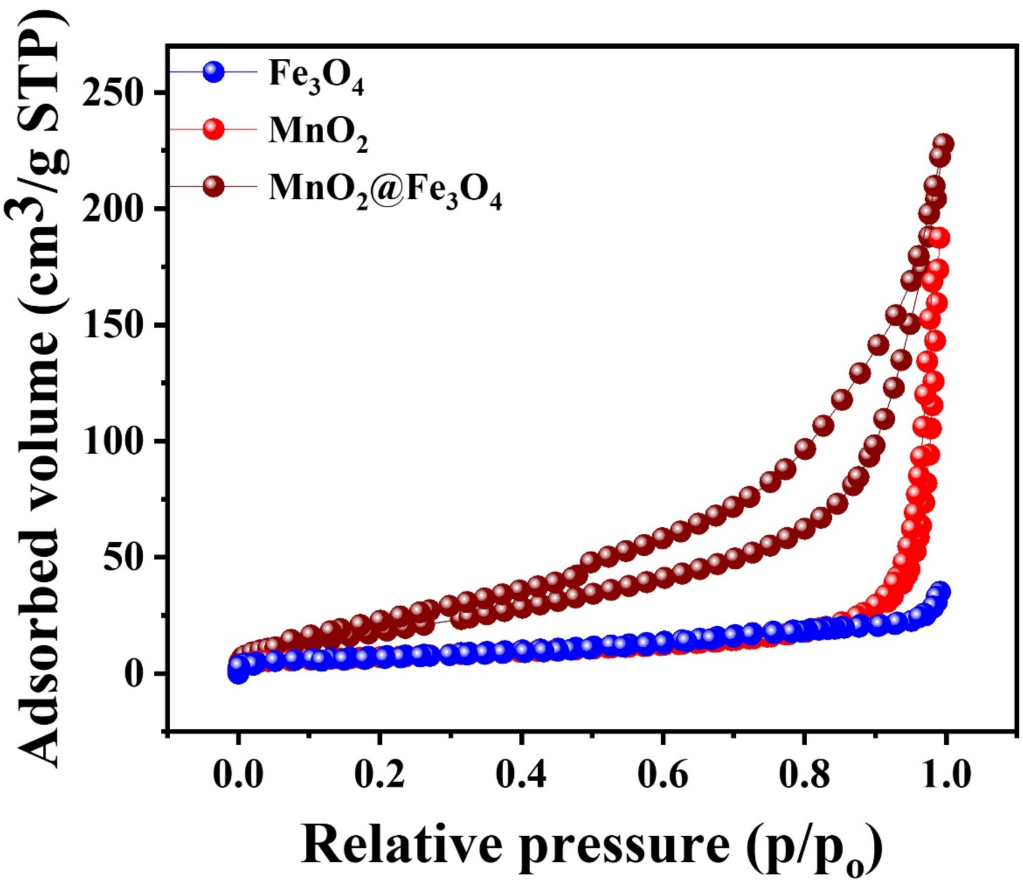

Figure S1. N_2 ads/des isotherms of the pristine Fe_3O_4, pristine MnO_2 and MnO_2@Fe_3O_4 nanoflower like structure.

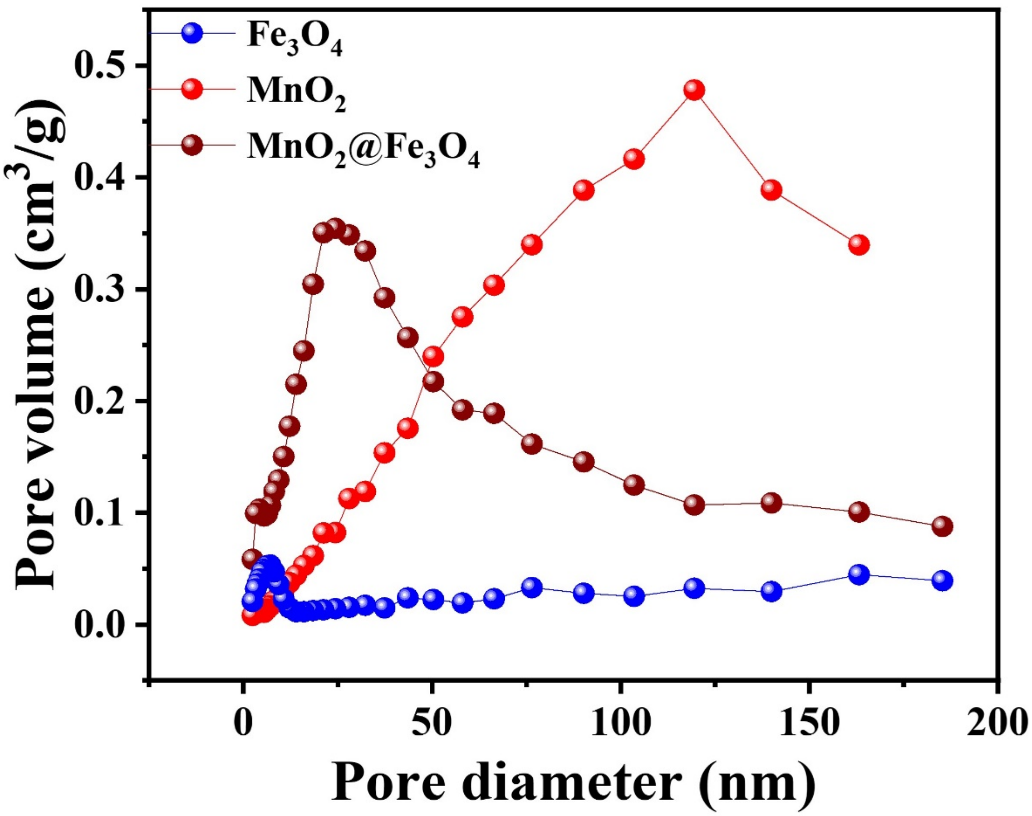

Figure S2. BJH curves of the pristine Fe_3O_4, pristine MnO_2 and MnO_2@Fe_3O_4 nanoflower like structure.

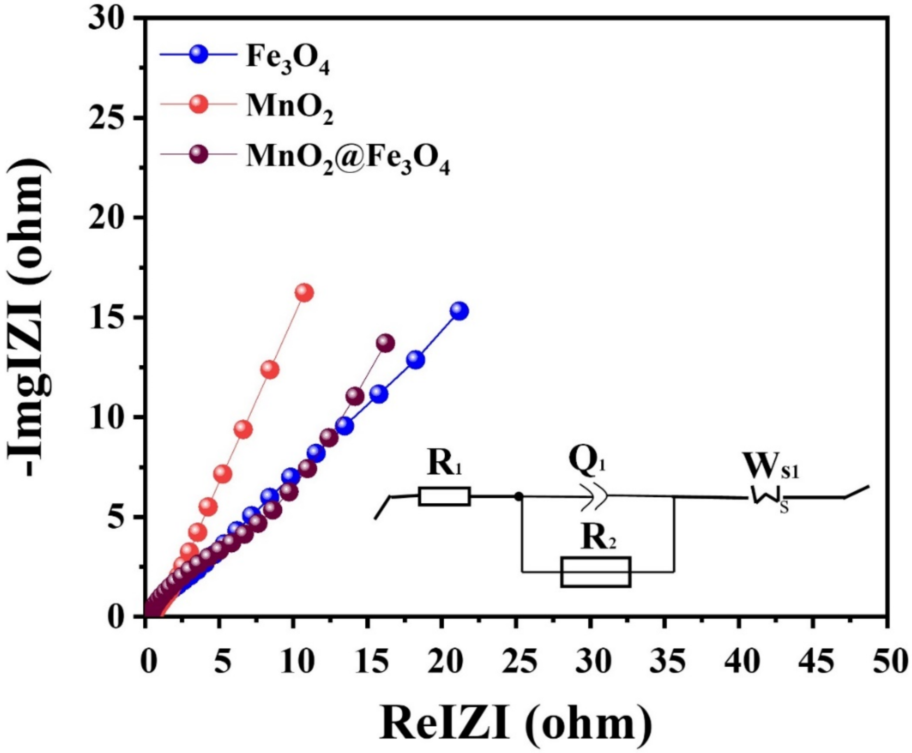

Figure S3. Nyquist plot of the pristine Fe_3O_4, pristine MnO_2 and MnO_2@Fe_3O_4 nanoflowers.

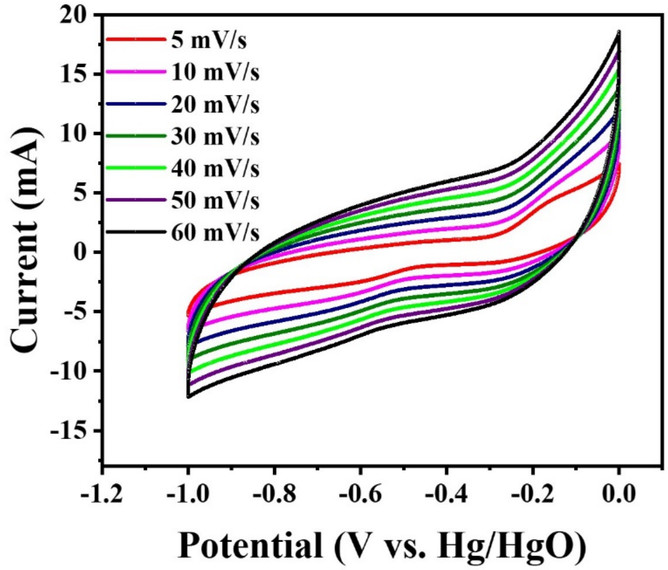

Figure S4. CV for the activated carbon at various scan rates in the potential range from -1.0 V to 0 V.

.

S5. Calculations for the loading mass

The mass ratio was calculated from the following equations to obtain charge balance

$$\frac{m_+}{m_-} = \frac{C_{s-} \times \Delta V}{C_{s+} \times \Delta V} \qquad (1)$$

where m+ and m- are masses on positive (cathode) and negative (anode) electrodes of the ASC, Cs+ and Cs− are specific capacitances of the electrode materials in the potential windows of ΔV- and ΔV+, respectively, measured against a reference electrode in the three electrode configurations. The mass loading ratio of the positive and negative electrodes was estimated as ~5.7, according to eq 1. Approximately 1.5 mg of negative electrode (AC) and 0.9 mg of positive electrode (MnO_2@Fe_3O_4 nanoflower) were used to maintain the charge neutrality of ASC. Electrochemical assessment of ASC was carried out on the basis of total mass loading on both electrodes. In this study, both electrodes were obtained using the three-electrode system over a potential window of 0 to 0.6 V for the MnO_2@Fe_3O_4 nanoflower cathode and 0 to -1.0 V for the AC anode electrode, which collectively provide a large potential window of upto 1.6 V for the MnO_2@Fe_3O_4//AC nanoflower ASC device. Therefore, the initial voltage is 0 and final provided voltage is 1.6. So, ΔV = 1.6-0 = 1.6 V, which is fixed for our study.

Table S1. Comparison of specific capacitance of $MnO_2@Fe_3O_4$ nanoflowers reported to date with those in the present study.

Electrode materials	Electrolytes	Potential window (V)	Specific capacitance/ current density	Ref.
$MnO_2@Fe_3O_4$ nanoflower	**3 M KOH**	**0-0.6**	**1651 $F.g^{-1}$ at 1 $A.g^{-1}$**	**Present work**
Co_3O_4@CNF	3 M KOH	-0.2-0.6	789.9 $F.g^{-1}$ at 1 $A{\cdot}g^{-1}$	[1]
$ZnMn_2O_4$/C	6 M KOH	0-1.2	589 $F.g^{-1}$ at 1 $A{\cdot}g^{-1}$	[2]
ZnO/MnO	1 M Na_2SO_4	0-0.8	14 mF/cm^2 at 0.1 mA/cm^2	[3]
ZnO/MnO_2 nanowires	1 M Na_2SO_4	0-0.9	501 $F.g^{-1}$ at 2 $A{\cdot}g^{-1}$	[4]
$ZnMn_2O_4$/carbon	6 M KOH	-1-(-0.3)	105 $F.g^{-1}$ at 0.3 $A{\cdot}g^{-1}$	[5]
ZnO nanocones	1 M KOH	0.1-0.6	236 $F.g^{-1}$ at 1 $A{\cdot}g^{-1}$	[6]
NCA/Co_3O_4	6 M KOH	-0.05-0.45	616 $F{\cdot}g^{-1}$ at 1.2 $A{\cdot}g^{-1}$	[7]
ZnO/MnO_2	0.5 M Na_2SO_4	0-0.8	262 $F{\cdot}g^{-1}$ at 0.2 $A{\cdot}g^{-1}$	[8]
ZnO/MnO nanoflowers	1 M Na_2SO_4	0-0.9	556 $F{\cdot}g^{-1}$ at 1 $A{\cdot}g^{-1}$	[9]
ZnO-/core like MnO_2	1 M Na_2SO_4	0-0.8	221 $F{\cdot}g^{-1}$ at 0.5 $A{\cdot}g^{-1}$	[10]
ZnO/MnO_2 core/shell	1 M Na_2SO_4	-0.2-0.8	424 $F{\cdot}g^{-1}$ at 0.5 $A{\cdot}g^{-1}$	[11]
ZnO/MnO_2 nanocables	0.5 M Na_2SO_4	0-0.9	613 $F{\cdot}g^{-1}$ at 1.2 $A{\cdot}g^{-1}$	[11]
Ni-Co selenide	6 M KOH	0 to 0.6	742.4 $F{\cdot}g^{-1}$ at 1 mA cm^{-2}	[12]
$NiCo_2O_4$	6 M KOH	-0.2 to 0.6	225 C. g^{-1} at 0.5 A g^{-1}	[13]

Reference:

[1] I. Rabani, J. Yoo, H.-S. Kim, S. Hussain, K. Karuppasamy, and Y.-S. Seo, "Highly dispersive Co 3 O 4 nanoparticles incorporated into a cellulose nanofiber for a high-performance flexible supercapacitor," *Nanoscale,* vol. 13, no. 1, pp. 355-370, 2021.

[2] Z. Zhu, Z. Wang, Z. Yan, R. Zhou, Z. Wang, and C. Chen, "Facile synthesis of MOF-derived porous spinel zinc manganese oxide/carbon nanorods hybrid materials for supercapacitor application," *Ceramics International,* vol. 44, no. 16, pp. 20163-20169, 2018.

[3] C. J. Raj *et al.*, "Two-dimensional planar supercapacitor based on zinc oxide/manganese oxide core/shell nano-architecture," *Electrochimica Acta,* vol. 247, pp. 949-957, 2017.

[4] S. Li *et al.*, "Three-dimensional MnO2 nanowire/ZnO nanorod arrays hybrid nanostructure for high-performance and flexible supercapacitor electrode," *Journal of Power Sources,* vol. 256, pp. 206-211, 2014.

[5] C.-K. Sim, S. R. Majid, and N. Z. Mahmood, "Durable porous carbon/ZnMn2O4 composite electrode material for supercapacitor," *Journal of Alloys and Compounds,* vol. 803, pp. 424-433, 2019.

[6] X. He, J. E. Yoo, M. H. Lee, and J. Bae, "Morphology engineering of ZnO nanostructures for high performance supercapacitors: enhanced electrochemistry of ZnO nanocones compared to ZnO nanowires," *Nanotechnology,* vol. 28, no. 24, p. 245402, 2017.

[7] G. Sun, L. Ma, J. Ran, X. Shen, and H. Tong, "Incorporation of homogeneous Co 3 O 4 into a nitrogen-doped carbon aerogel via a facile in situ synthesis method: implications for high

performance asymmetric supercapacitors," *Journal of Materials Chemistry A,* vol. 4, no. 24, pp. 9542-9554, 2016.

[8] W. Li *et al.*, "Urchin-like MnO2 capped ZnO nanorods as high-rate and high-stability pseudocapacitor electrodes," *Electrochimica Acta,* vol. 186, pp. 1-6, 2015.

[9] E. Samuel, B. Joshi, Y.-i. Kim, A. Aldalbahi, M. Rahaman, and S. S. Yoon, "ZnO/MnO x nanoflowers for high-performance supercapacitor electrodes," *ACS Sustainable Chemistry & Engineering,* vol. 8, no. 9, pp. 3697-3708, 2020.

[10] Y. Zhao, P. Jiang, and S.-S. Xie, "ZnO-template-mediated synthesis of three-dimensional coral-like MnO2 nanostructure for supercapacitors," *Journal of power sources,* vol. 239, pp. 393-398, 2013.

[11] M. Huang *et al.*, "Hierarchical ZnO@ MnO2 core-shell pillar arrays on Ni foam for binder-free supercapacitor electrodes," *Electrochimica Acta,* vol. 152, pp. 172-177, 2015.

[12] Y. Wang *et al.*, "Ni–Co Selenide Nanosheet/3D Graphene/Nickel Foam Binder-Free Electrode for High-Performance Supercapacitor," *ACS applied materials & interfaces,* vol. 11, no. 8, pp. 7946-7953, 2019.

[13] H. Fu *et al.*, "Designed formation of NiCo2O4 with different morphologies self-assembled from nanoparticles for asymmetric supercapacitors and electrocatalysts for oxygen evolution reaction," *Electrochimica Acta,* vol. 296, pp. 719-729, 2019.